THE JOURNAL OF PHYSICAL CHEMISTRY C

Article

pubs.acs.org/JPCC

Surface Reduction Mechanism of Cerium−Gallium Mixed Oxides with Enhanced Redox Properties

Julia Vecchietti,[†] Sebastián Collins,[†] Wenqian Xu,[‡] Laura Barrio,[‡,○] Darío Stacchiola,[‡] Mónica Calatayud,[§,∥] Frederik Tielens,[⊥] Juan José Delgado,[#] and Adrian Bonivardi*[,†]

[†]Instituto de Desarrollo Tecnológico para la Industria Química, Universidad Nacional del Litoral and CONICET, Güemes 3450, 3000, Santa Fe, Argentina

[‡]Department of Chemistry, Brookhaven National Laboratory, Upton, New York 11973, United States

[§]Laboratoire de Chimie Théorique, Université Pierre et Marie Curie and CNRS, UMR 7616, F-75005, Paris, France

[∥]Institut Universitaire de France

[⊥]Laboratoire de Réactivité de Surface, Université Pierre et Marie Curie and CNRS, UMR 7197, F-75005 Paris, France

[#]Departamento de Ciencias de los Materiales, Ingeniería Metalúrgica y Química Inorgánica, Facultad de Ciencias, Universidad de Cádiz, Puerto Real, E11510, Spain

ABSTRACT: The doping of CeO_2 with different types of cations has been recognized as a significant factor in controlling the oxygen vacancies and improving the oxygen mobility. Thus, the catalytic properties of these materials might be determined by modifying the redox properties of ceria. A combined experimental and theoretical study of the redox properties of gallium-doped cerium dioxide is presented. Infrared spectroscopy and time-resolved X-ray diffraction were used for temperature programmed reduction (H_2) and oxidation (with O_2 and H_2O) studies. Additionally, X-ray absorption near edge spectroscopy shows that only Ce^{4+} is reduced to Ce^{3+} in the ceria−gallia mixed oxides when annealed up to 623 K. The oxygen storage capacity (OSC) measurements show a pronounced enhancement on the reduction of ceria by gallium doping. Theoretical calculations by density functional theory (DFT) confirm the higher reducibility of gallium-doped ceria oxides and give a molecular description of the stabilization of the doped material. On the basis of infrared spectroscopic measurements, a novel mechanism is proposed for the surface reduction of Ce^{4+} to Ce^{3+} where Ga−H species are suggested to be directly involved in the process. In addition, the reoxidation by H_2O was precluded in the gallium-doped ceria oxide.

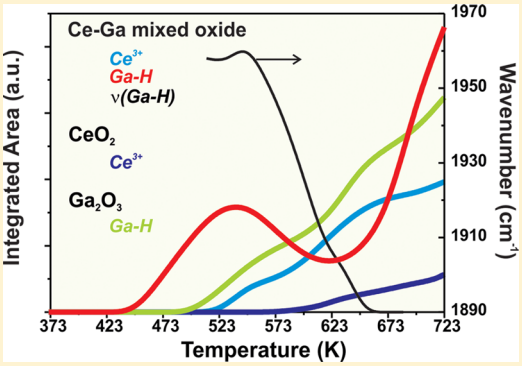

INTRODUCTION

Cerium dioxide is widely used as a component or an active phase in numerous redox catalytic processes.[1] Two major reasons justify the relevance in catalysis of ceria, the ability to rapidly exchange oxygen with the chemical environment, with reversible shift of the cerium redox state (Ce^{4+}/Ce^{3+}), and the mobility of oxygen exhibited by its fluorite-type structure. Doping ceria with alio-cations is known to be an efficient and versatile way of modulating the textural, structural, and chemical properties of the pure oxide.[2,3]

Catalytic systems containing highly dispersed gold or platinum supported on CeO_2 or modified-ceria have shown the most remarkable catalytic properties for hydrogen purification through the water gas shift reaction (WGSR) and the preferential oxidation of CO (PROX).[4−7] For such catalytic applications, the optimum size of gold particles must be less than 5 nm.[8−10] Such particle sizes can be achieved by a careful control of the preparation conditions and storage of the catalysts.[11] The stabilization of structures involving Ce^{3+} has proven to dramatically improve both metal dispersion and catalytic activity of ceria containing catalysts.[12] However, some authors have postulated that the deactivation of some of these cerium based systems can be attributed to the formation of strongly adsorbed carbonate species on ceria.[13] Therefore, the tuning of the surface acid−base properties could be envisaged as an improvement in the stability of the catalysts.

In a previous study, we investigated the synthesis of a series of Ce−Ga mixed oxides and found that gallium-doped ceria modifies simultaneously the redox and acid−base properties of CeO_2.[14,15] The structural analysis by X-ray diffraction (XRD) of a set of Ce−Ga materials in a wide range of compositions (Ce/Ga atomic ratio = 95/5, 90/10, 80/20, and 75/25),[14,15] together with nanostructural analysis and chemical composition by high-resolution electron microscopy (HREM) and energy-dispersive spectroscopy (EDS) on a sample Ce/Ga = 80/20, allowed us to verify that it is possible to incorporate

Received: January 9, 2013
Revised: April 3, 2013
Published: April 3, 2013

   dx.doi.org/10.1021/jp400285b | J. Phys. Chem. C 2013, 117, 8822−8831

homogeneously Ga^{3+} cations to the fluorite-type structure of ceria.[16] Temperature-programmed reduction with both H_2 and CO showed that the redox behavior was noticeably enhanced in the gallium-doped ceria materials as compared with the pure ceria.[14,16]

In order to gain insight on the origin of the enhanced reducibility of the mixed oxides, the redox properties of the oxides are here evaluated *in situ* using time-resolved infrared spectroscopy (IR) by transmittance and diffuse reflectance (DRIFT) modes, time-resolved X-ray diffraction, and X-ray absorption near edge spectrometry (XANES). The ultimate oxygen storage capacity (OSC) of the materials was also measured. Moreover, the nature of the better reducibility of the gallium-doped materials was characterized by periodic density functional theory (DFT) calculations.

EXPERIMENTAL AND THEORETICAL METHODS

Materials. Ceria, gallia, and cerium−gallium mixed oxide were prepared from high purity grade nitrate salts (Sigma-Aldrich, 99.99% Ce and 99.999% Ga). Three mixed oxide samples with nominal atomic ratios of Ce to Ga equal to 95/5, 80/20, and 75/25 (hereafter, Ce95Ga05, Ce80Ga20, and Ce75Ga25, respectively) were prepared.

Details of the material preparation methods have been previously reported.[14] Briefly, CeO_2, Ga_2O_3, and mixed cerium/gallium materials were prepared by precipitation in ammonia solution (pH 8.5) of the respective nitrate dissolved in water, and ethanol in the case of gallium 3+ cations alone, to give materials with a specific surface, measured by the BET method, equal to 62, 94, 100, 100, and 76 m^2/g for CeO_2, Ce95Ga05, Ce80Ga20, Ce75Ga25, and Ga_2O_3, respectively. Additionally, the grain size of ceria domains in the oxides, determined by XRD, was 16.9, 9.0, 5.8, and 4.2 ± 0.5 nm from pure CeO_2 to Ce75Ga25 as expected for the increase of gallium content into the ceria matrix.

OSC Measurements. Ultimate oxygen storage capacity measurements were conducted by thermogravimetric analysis with a TA thermobalance, model Q-600. Typically, 100 mg of sample was submitted to the following cleaning pretreatment: (i) reduction under H_2 flow from 298 up to 773 K (10 K/min) for 15 min, (ii) purge under He flow at 773 K (15 min), (iii) oxidation under O_2 flow at 773 K (15 min), (iv) cooling under O_2 flow from 773 to 473 K, and (v) purge under He flow at 473 K (15 min). After the cleaning pretreatment, a flow of 5% H_2/Ar was admitted at 473 K and the temperature was increased by steps of 100 K (1 h each), with a heating rate equal to 10 K/min. All gas flows were set to 60 cm^3/min.

TPR and TPO Experiments by IR Spectroscopy. Temperature programmed reduction (with H_2) and oxidation (with O_2 and H_2O) experiments were performed (TPR and TPO, respectively) by *in situ* transmission IR spectroscopy using a Nicolet 8700 FTIR spectrometer operated with a Hg−Cd−Te detector.

Self-supported wafers of each solid (approximately 30 mg/cm^2) were placed in an electrically heated glass flow-through cell fitted with CaF_2 windows. Each sample was pretreated with a cleaning protocol similar to the one described above in the OSC measurements, but purging and cooling processes (steps ii, iv, and v) were done under vacuum (instead of He flow). Next, H_2-TPR measurements were performed under a flow of pure H_2 (50 cm^3/min) by heating the IR cell from 298 up to 723 K (10 K/min). Then, after evacuating the cell and cooling the sample to 298 K, H_2O-TPO or O_2-TPO measurements were carried out by (a) admitting a pulse of gaseous water (550 μmol) into the cell or (b) using an O_2 flow equal to 50 cm^3/min, and heating the sample to 723 K (10 K/min) in either case.

IR spectra were taken consecutively with an average of 25 scans (acquisition time = 5 s) and a resolution equal to 4 cm^{-1}.

Isothermal Reduction Studies by IR Spectroscopy. The isothermal reduction with H_2 (30 cm^3/min) was studied at 523 and 623 K by means of step experiments, on previously oxidized samples by IR in DRIFT mode. A Harrick high-temperature cell (model HCV-DRP, Praying Mantis) with KBr windows located in the sample compartment of the above-mentioned IR spectrophotometer was used. The experimental sample pretreatment was as follows: heating under H_2 flow from 298 to 623 K (15 K/min), followed by isothermal treatment at 623 K with the H_2−He−H_2−He−O_2−He gas sequence (10 min under the flow of each gas). Subsequently, isothermal reduction measurement at 623 K under H_2 flow was performed (first step experiment). Then, the sample was oxidized by O_2 and next the cell was purged under He, at 623 K. Finally, the sample was cooled and the isothermal reduction experiment at 523 K was conducted (second step experiment). Gas flow was equal to 30 cm^3/min in any case. Our DRIFT cell behaves as a continuous stirred tank reactor (CSTR) with a residence time equal to 30 s for the volumetric flow employed in the step experiments, which allowed reproducible IR results. The temperature of the sample into the cup of the DRIFT cell was calibrated under gas flow by using a thermocouple inserted into the sample holder loaded with CeO_2. IR spectra were recorded as described in the previous section.

TPR and TPO Experiments by XRD. The structure of the Ce−Ga mixed oxides was evaluated under H_2-TPR, O_2-TPO, and H_2O-TPO experiments by *in situ* time-resolved XRD. These tests were carried out at the beamline X7B (λ = 0.3196 Å) of the National Synchrotron Light Source at Brookhaven National Laboratory. The cell used consists of a quartz capillary (diameter = 1 mm) that allows gas flow through the sample. The cell was heated by a resistance coil, and the temperature was monitored by a thermocouple inserted into the capillary close to the sample. The gas outlet was connected to a mass spectrometer (QMS, Stanford Research Systems). A Perkin-Elmer amorphous silicon two-dimensional detector was used for the acquisition of the diffractograms. Sequential Rietveld analysis was performed with the program GSAS using a LaB_6 reference.[17]

XAFS Study. The reduction of the supports was also analyzed by *in situ* X-ray absorption fine structure spectrometry (XAFS). Ga K-edge and Ce L_{III}-edge XANES (X-ray absorption near edge structure) spectra were collected under 5% H_2/He flow at 298, 423, 523, and 623 K at the beamline X19A of the NSLS. The same cell was used for the XANES experiments as that for *in situ* XRD, except that the sample was loaded into a kapton capillary and heated with hot air. The X-ray absorption spectra were taken repeatedly in the "fluorescence-yield mode" using an implanted planar silicon (PIPS) water-cooled detector. XAFS data were analyzed using the Athena and Artimis programs.[18]

DFT Calculations. The VASP code[19−21] was used to determine total energies of pure ceria, pure gallia, and Ce75Ga75 model systems. The Perdew−Burke−Ernzerhof functional was employed as implemented in the code to solve the Kohn−Sham equations. Projector-augmented wave (PAW) generated pseudopotentials[22,23] replaced the core electrons

dx.doi.org/10.1021/jp400285b | J. Phys. Chem. C 2013, 117, 8822−8831

(Ce, Ga_d, and O PAW_PBE as given in the VASP library), and the valence electrons were explicitly treated with a plane wave basis set with a 400 eV cutoff. A *k*-points mesh with points at a distance of ~0.05 $Å^{-1}$ sampled the Brillouin zone. Geometrical optimizations of the stoichiometric systems were performed in two steps: first, the atoms were allowed to relax, and second, the volume of the cell was relaxed (for the latter, a cutoff of 500 eV was used). Then, the cell was kept fixed to the optimized cell parameter values and an oxygen atom was removed, allowing all the atoms to relax (cutoff 400 eV). Different nonequivalent lattice oxygen sites were tested. The conjugate-gradient algorithm is employed to search minimum energy structures within a threshold of 10^{-4} eV for the electronic loops and 10^{-3} eV for the ionic relaxation. Spin polarized formalism is used for the calculation of reduced structures. The cubic fluorite structure was used to model pure ceria and doped Ce75Ga25 (2 × 2 × 2 unit cell). The beta-gallia (1 × 2 × 2) unit cell was used to model pure gallia. These supercells allow the comparison of the oxygen vacancy formation energy values for similar concentrations of vacancies.

RESULTS AND DISCUSSION

Reduction by *in Situ* XANES. The reduction state of the cerium and gallium cations in the different bulk oxides was investigated by *in situ* XANES experiments using hydrogen as a reducing agent. The oxidation state of the cerium was studied by analyzing the changes on the Ce L_{III} edge XANES spectra of CeO_2 and Ce80Ga20 samples during the reduction process (Figure 1). Pure CeO_2 and Ce80Ga20 show twin absorption

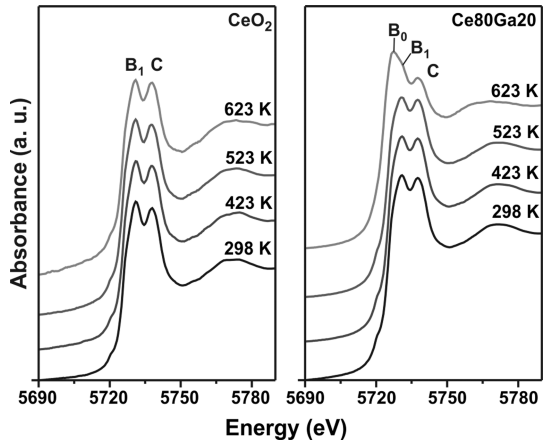

Figure 1. Ce L_{III}-edge XANES spectra of CeO_2 and Ce80Ga20 under 5% H_2/He flow at different temperatures.

peaks, which were labeled B_1 and C (at 5731 and 5738 eV, respectively) under H_2 below 623 K, and are assigned to the predominance of Ce^{4+} species.[24,25] However, a new peak at approximately 5728 eV, which was named B_0 and is strongly overlapped with the B_1 peak, develops on the spectrum of the reduced Ce80Ga20 sample at 623 K (Figure 1). The development of B_0, together with a decrease of the C peak intensity, is a clear indication of a substantial reduction of Ce^{4+} to Ce^{3+}.[24,25] This behavior, the appearance of the B_0 peak and the C peak declining its intensity, is not observed in pure ceria, which is congruent with the higher cerium reducibility in the mixed-oxide samples detected during the OSC and temperature-programmed reduction experiments using IR spectroscopy (see below).

Figure 2 shows the spectra of the Ga K-edge for the cerium–gallium mixed oxides (that is, the Ce95Ga05 and Ce80Ga20

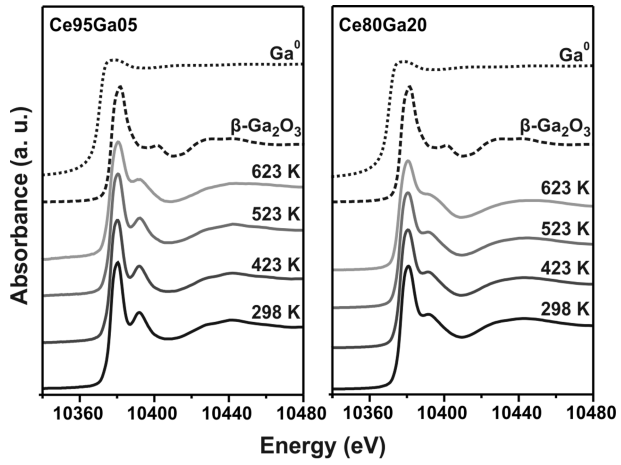

Figure 2. Ga K-edge XANES spectra of Ce95Ga05 and Ce80Ga20 under 5% H_2/He flow at different temperatures. For comparison, the reference spectra of β-Ga_2O_3 (dashed trace) and metallic gallium, Ga^0 (dotted trace), are included.

samples) at different reduction temperatures. The direct comparison of the XANES spectra of the gallium-doped ceria samples with those of the reference compounds, metallic gallium (Ga^0) and pure β-Ga_2O_3, reveals that gallium is mainly present as Ga^{3+} under H_2 up to 623 K; in other words, Ga^{3+} is not significantly reduced to be detected by XANES.

Oxygen Storage Capacity. To obtain quantitative information about the redox properties of the materials, the total or ultimate oxygen storage capacity (OSC) of the synthesized oxides was measured.

Figure 3 shows the results of OSC as the evolution of the amount of released oxygen per mass of CeO_2 with the increase

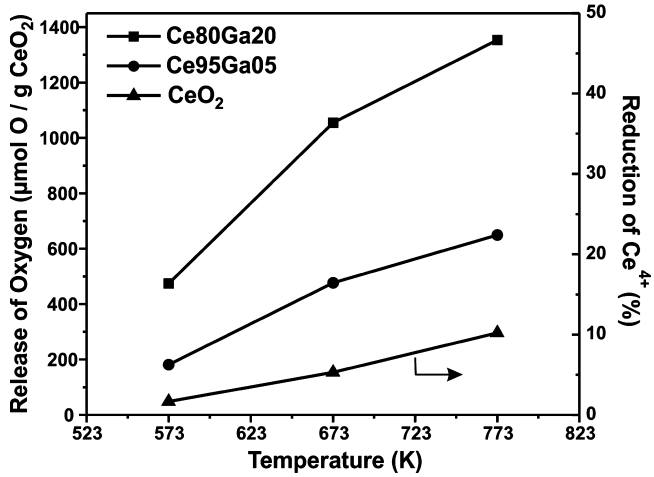

Figure 3. Oxygen storage capacity (OSC) versus the temperature of reduction for pure CeO_2 and cerium–gallium mixed oxides (Ce95Ga05 and Ce80Ga20).

of temperature. It can be observed that the reducibility of pure ceria increases from 1.6 to 10% when annealed from 573 to 773 K. Since no CeO_2 bulk reduction was detected by *in situ* XANES measurements on CeO_2, it is suggested that mainly

dx.doi.org/10.1021/jp400285b | J. Phys. Chem. C 2013, 117, 8822–8831

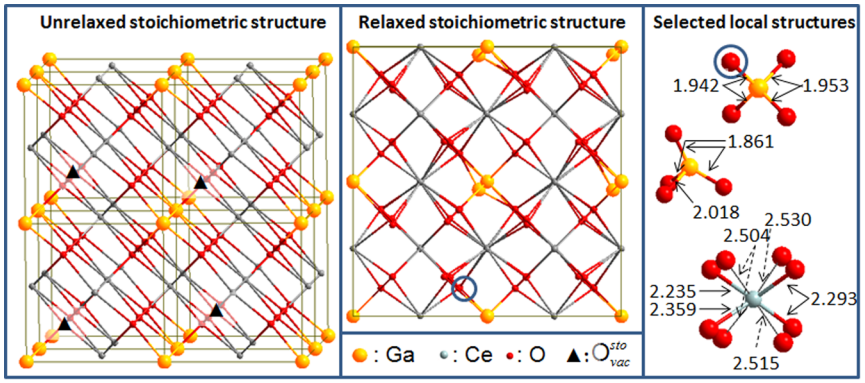

Figure 4. The supercell used for modeling the Ce75Ga25 bulk material. It is built from a pure ceria $2 \times 2 \times 2$ $Ce_{32}O_{64}$ supercell. Then, four O atoms linking Ce and Ga sites have been removed with respect to the stoichiometry of the doped material; their position in the cell is displayed as triangles. Left: starting point (pure ceria positions for all atoms). Middle: optimized structure. Right: the local environment for selected atoms is also shown, distances in Å.

Table 1. Total Energy (TOTEN) and Oxygen Vacancy Energy Formation (E_{vac}) Calculated with eq 1 for Pure Ceria, Gallia, and the Ce75Ga25 Model Systems[a]

system	stoichiometric formula	TOTEN	$N_\alpha - N_\beta$	reduced formula	TOTEN	$N_\alpha - N_\beta$	E_{vac}
O		−1.89	2				
O_2		−9.86	2				
CeO_2	$Ce_{32}O_{64}$	−840.79	0	$Ce_{32}O_{63}$	−832.63	2	3.23
Ga_2O_3	$Ga_{32}O_{48}$	−483.69	0	$Ga_{32}O_{47}$	−474.75	0	4.00
Ce75Ga25	$Ce_{24}Ga_8O_{60}$	−737.60	0	$Ce_{24}Ga_8O_{59}$	−730.12	2	2.54

[a]The spin state is given by the number of unpaired electrons, $N_\alpha - N_\beta$ (0 indicates a closed-shell system, 2 means a triplet).

surface Ce^{4+} species are reduced to Ce^{3+} in pure ceria below 673 K.

By doping CeO_2 with 5 and 20% gallium, the percentage of Ce^{4+} reduction at 573 K is 4 and 10 times higher on the mixed oxides (6.3 and 16% for Ce95Ga05 and Ce80Ga20, respectively) as compared with pure ceria (1.6%). The percentage amount of reduced Ce^{4+} was obtained by assuming that all the Ce^{4+} is reduced to Ce^{3+} under 673 K, that is, assuming that Ga^{3+} is not significantly reduced, as was observed in the XAFS experiments up to 623 K. When the temperature is increased over 673 K, the extent of the sample reducibility also increases, reaching values of 649 and 1353 μmol of O/g_{CeO_2} for the Ce95Ga05 and Ce80Ga20 samples, respectively. Thus, the cerium−gallium mixed oxides are approximately 2- and 4-fold more reducible (for Ce95Ga05 and Ce80Ga20, respectively) than pure CeO_2 at the highest temperature employed in these experiments (297 μmol of O/g_{CeO_2}).

It can then be concluded that (i) most of the weight loss of the sample in the hydrogen atmosphere can be attributed to the easier release of oxygen in the gallium-doped ceria samples and (ii) mainly surface Ce^{4+} is reduced to Ce^{3+} below 673 K.

DFT Calculations. The cost of formation of an oxygen vacancy is used as a reactivity index for the reducibility, and is calculated from the total energy of the stoichiometric, reduced, and the free O_2 optimized structures as follows:

$$E_{vac} = E_{stoichiometric} - [E_{reduced} + {}^1/_2 E_{O_2}] \quad (1)$$

The lower the positive value, the easier to form an oxygen vacancy and the more reducible is the material. A supercell with composition Ce24Ga8O60 is used to model the bulk Ce75Ga25 material and is displayed in Figure 4. This composition allows keeping the formal oxidation states of the ions in the stoichiometric lattice (Ce^{4+}, Ga^{3+}, O^{2-}). The reduced materials were modeled by removing one lattice oxygen; different possibilities were tested, and only the most stable is described for the sake of clarity. Table 1 summarizes the results obtained for the studied systems. The cost of formation of an oxygen vacancy in pure CeO_2 is found to be 3.23 eV, which is in agreement with previous results.[26] The value obtained for pure gallia is 4.00 eV. The Ce75Ga25 model presents a calculated E_{vac} value of 2.54 eV. These results clearly show that the doped material is more reducible than the pure ones in agreement with the OSC and XANES measurements.

An analysis of the geometrical parameters of the doped *stoichiometric* system shows that the presence of gallium strongly modifies the local environment of the lattice ions, in agreement with previous calculations on a more diluted doped system.[27] Thus, Ga sites after optimization become tetrahedral instead of cubic in the fluorite structure. The GaO distances in the doped structure are of three types: short (1.86−1.95 Å), medium (2.02−2.22 Å), and large (2.49−2.53 Å); for comparison, $Ga_{tet}O$ distances found for β-gallia are 1.85 Å. Also, cerium centers are surrounded by two different oxygen sites, leading to short CeO (2.20−2.30 Å) and long CeO (2.50−2.53 Å) compared to the fluorite CeO distance of 2.36 Å. Oxygen sites present in the Ce75Ga25 model are 3-fold or 4-fold coordinated. With regard to the gallium-doped *reduced* system, an important relaxation phenomenon takes place upon the removal of the oxygen atom (displayed in Figure 5). When the oxygen atom is removed, the Ga atom moves in an umbrella-type displacement and binds to another oxygen behind. The lattice seems then to compensate for the absence of an oxygen atom. The flexibility of this movement may be the origin of an easy reduction/reoxidation or diffusion process.

The electronic structure of a reduced oxide is important for the comprehension of the reduction mechanism. The formation

dx.doi.org/10.1021/jp400285b | J. Phys. Chem. C 2013, 117, 8822−8831

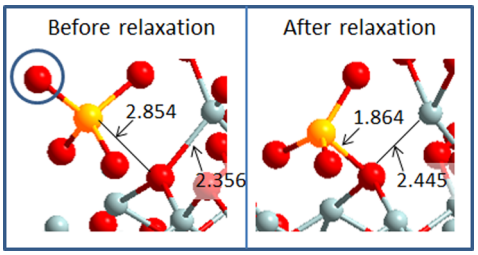

Figure 5. Local structure of the reduced Ce75Ga25 model before relaxation (left) and after relaxation (right). The oxygen atom removed (circle), to obtain the reduced structure, induces an umbrella movement of the Ga atom which binds to an oxygen site behind. Distances are in Å.

of an oxygen vacancy in a metal oxide leaves two electrons that may be localized in a lattice point (F center) or may be transferred to lattice cations.[28,29] The former case involves a closed-shell system and is found for irreducible metal oxides like Ga_2O_3. The latter involves an open-shell triplet and is the case for reducible metal oxides like CeO_2 (reduction of two Ce^{4+} to Ce^{3+}). The mixed Ce75Ga25 system behaves like ceria, and the formation of an oxygen vacancy leads to two reduction electrons occupying Ce4f states. This is again in agreement with the XANES results where only Ce^{4+} is reduced to Ce^{3+}, and bulk Ga^{3+} species remain fully oxidized at temperatures lower than 673 K.

Reduction and Oxidation Measurements by IR Spectroscopy and *in Situ* XRD. During the infrared measurements of TPR, TPO, and isothermal reduction, two characteristic IR bands were analyzed: a peak at 2127 cm^{-1}, which is assigned to the forbidden electronic transition $^2F_{5/2} \rightarrow {}^2F_{7/2}$ of Ce^{3+} cations,[30−33] and a band at approximately 2000 cm^{-1} attributed to the stretching mode of the Ga−H surface bond [ν(Ga−H)] in pure gallium oxides,[34,35] which is down shifted when gallium cations are incorporated into the fluorite structure of the ceria lattice.[14] In this way, it was possible to follow the steps of the redox process for the pure and mixed oxides as it is described below.

Temperature Programmed Reduction. Figure 6 shows an example of the thermal evolution of IR spectra in the 2300−1700 cm^{-1} region during the H_2-TPR for CeO_2, Ga_2O_3, and Ce75Ga25 samples. Due to the low signal-to-noise ratio for the IR band corresponding to the Ga−H stretching mode, only the results for the mixed oxide with the highest gallium loading (that is, Ce75Ga25) will be shown, but identical trends were obtained for the other two materials (Ce95Ga05 and Ce80Ga20).

It is clear that on pure ceria or gallia only the signal attributed to Ce^{3+} or Ga−H is observed, respectively. In the latter case, the γ-Ga_2O_3 develops two overlapped bands at 2003 and 1980 cm^{-1} assigned to the dissociative chemisorption of H_2 on surface gallium sites in tetrahedral [$\nu(Ga^{IV}-H)$] and octahedral [$\nu(Ga^{VI}-H)$] coordination, respectively.[34]

However, two bands were registered during the reduction of the mixed oxide under a hydrogen atmosphere: the band corresponding to Ce^{3+} and one that shifted from 1960 to 1890 cm^{-1} after the temperature increase from 523 to 673 K. The assignment of the latter band to ν(Ga−H) in the mixed oxide was confirmed by switching the H_2 flow to D_2 flow at 723 K. Thus, the band at 1890 cm^{-1} disappeared and a new band at 1350 cm^{-1} showed up, which is congruent with the expected wavenumber ratio due to the isotopic exchange of Ga−H to Ga−D (this value is proportional to the square root of the reduced mass ratio of Ga−D to Ga−H, that is, 1.40).

The thermal progress of the intensity of the main IR bands above-mentioned is shown in Figure 7. Several features can be highlighted from this figure, which we suggest are associated to different steps of the Ce−Ga mixed oxide reduction by molecular hydrogen and described in detail below.

First, it is possible to observe that the reduction of Ce^{4+} to Ce^{3+} is detected at a lower temperature on the cerium−gallium mixed oxide than on pure ceria (523 versus 573 K onset temperatures, respectively). Furthermore, the significantly higher intensity of the IR peak due to Ce^{3+} on Ce75Ga25 as compared to CeO_2, at all temperatures, indicates the greater degree of reduction of Ce^{4+} on this mixed oxide sample with the highest content of gallium cations, in accordance with the OSC and XANES results for Ce95Ga05 and Ce80Ga20 materials. Thus, in particular for the case of Ce75Ga25, the reducibility was verified by time-resolved XRD (Figure 8). The expansion of the lattice parameter at 673 K was 3 times higher

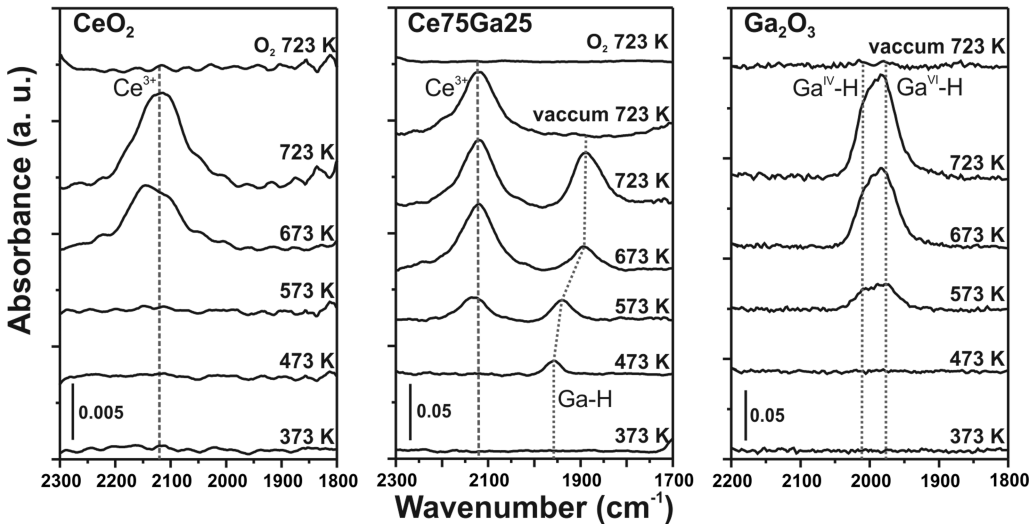

Figure 6. Evolution of the infrared spectra during the H_2-TPR experiments on CeO_2, Ce75Ga25, and Ga_2O_3. The upper traces show the effect of O_2 or vacuum over the Ce^{3+} ($^2F_{5/2} \rightarrow {}^2F_{7/2}$) or Ga−H signal [$\nu$(Ga−H)].

dx.doi.org/10.1021/jp400285b | J. Phys. Chem. C 2013, 117, 8822−8831

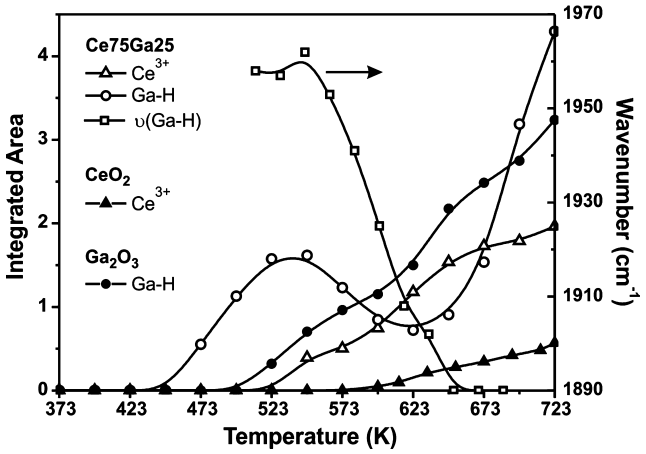

Figure 7. Thermal evolution of the concentration of the Ce^{3+} and Ga−H species and the IR wavenumber of the Ga−H bond stretching [ν(Ga−H)] during the H_2-TPR experiments on CeO_2, Ce75Ga25, and Ga_2O_3.

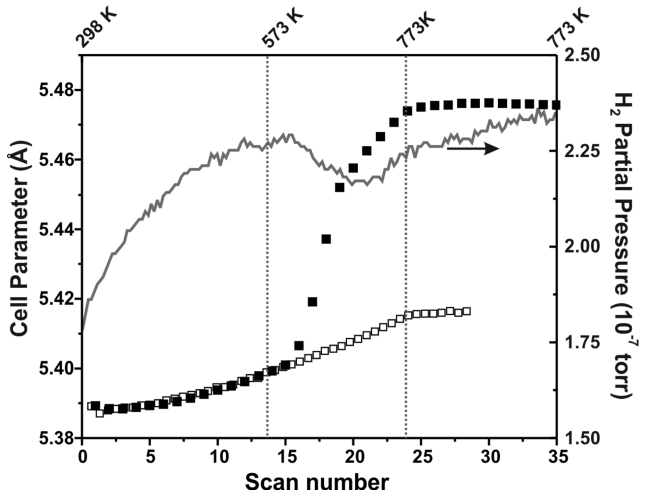

Figure 8. Thermal evolution of the lattice parameter measured by in situ XRD on Ce75Ga25 during the H_2-TPR experiment (filled squares) and under 5% O_2/He (open squares). The full line indicates the H_2 evolution.

(0.063 vs 0.020 Å) than that generated by heating the sample to the same temperature but in the absence of H_2 (see open squares in Figure 8). At the same time, the variation of the lattice parameter for pure CeO_2 was 0.021 at 673 K, which is practically equal to the estimated thermal expansion (the thermal expansion coefficient for ceria in air is (0.86−1.1) × 10^{-5} K^{-1} [36−38]). The further increase in the lattice parameter has been proven to be related to the reduction of ceria and the corresponding bigger size of the Ce^{3+} cations with respect to the Ce^{4+} cations.[5] It can be seen that this increase in the lattice parameter is accompanied by a decrease in the partial pressure of H_2, which confirms the bulk reduction of the cerium−gallium mixed oxide at the higher temperatures, that is, over 673 K. Therefore, the higher reducibility of the cerium−gallium mixed oxide as compared to CeO_2 is again verified in the highest gallium loading sample used in this work.

Second, in the case of pure gallium oxide, the concentration of Ga−H surface species increases with increasing temperature (Figure 7), while the ν(Ga−H) band positions at 2003 and 1980 cm^{-1} remained constant (Figure 6). The frequency of vibration of the Ga−H bond on the Ce−Ga oxide remains constant at 1960 cm^{-1} between 473 and 523 K, and then shifts to 1890 cm^{-1} when the temperature is raised to 723 K. Moreover, Figure 7 also shows that the integrated area of the ν(Ga−H) band in the Ce−Ga mixed oxide increases with increasing temperature up to 523 K, which is concurrent with the onset temperature that indicates the beginning of Ce^{3+} formation on said oxide. Then, the concentration of surface Ga−H species diminishes and reaches a minimum value at 623 K, to finally increase again at higher temperatures, as soon as the Ce^{3+} band levels off at T > 648 K. The strong shift of the Ga−H signal from 1960 to 1890 cm^{-1} mainly between 523 and 673 K underlined above suggests that the chemical environment of Ga−H sites has been modified by the presence of Ce^{3+} bringing a change in the strength of the Ga−H bond and/or that Ga^{3+} is progressively reduced to a lower and stable state of oxidation. The last possibility can be reasonably excluded, at least at temperatures lower than 623 K, because (i) XANES results were unable to show any reduction of the Ga^{3+} cations and (ii) DFT calculations indicate the preferential reduction of Ce^{4+} rather than that of the Ga^{3+} cations.

Thus, the peculiar variation in the concentration of Ga−H species on the cerium−gallium mixed oxide as a function of the temperature together with the wavenumber shift of the ν(Ga−H) peak and the enhanced reduction of Ce^{3+} as compared to pure ceria provide an indication that surface Ga−H species might be implicated in the initial step of the reduction of Ce^{4+} to Ce^{3+}.

Isothermal Reduction. In an effort to understand the mechanism involved in the reduction of the cerium−gallium mixed oxide, step experiments of isothermal reduction by H_2 were carried out in DRIFT mode. Two critical temperatures were chosen, that is, for the maximum and minimum of the Ga−H surface concentration detected during the non-isothermal IR experiments. The time evolutions of the IR signals during these reducing experiments at 523 and 623 K on the oxidized Ce75Ga25 sample are depicted in Figure 9. These isothermal traces together with the non-isothermal evolutions detailed above allow us to postulate the two-step mechanism

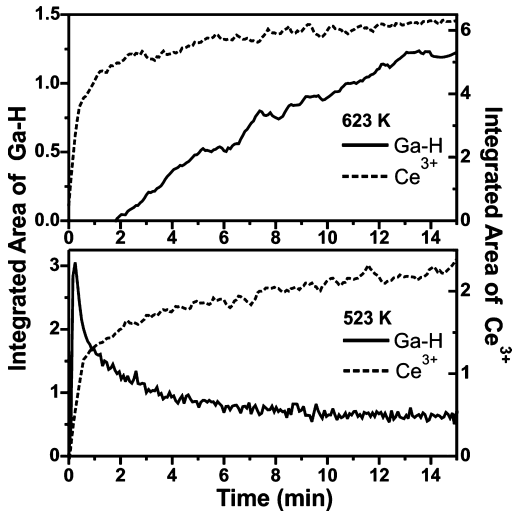

Figure 9. Isothermal evolution of the concentration of the Ce^{3+} and Ga−H species under flowing H_2 through the oxidized Ce75Ga25 sample in the DRIFT cell.

dx.doi.org/10.1021/jp400285b | J. Phys. Chem. C 2013, 117, 8822−8831

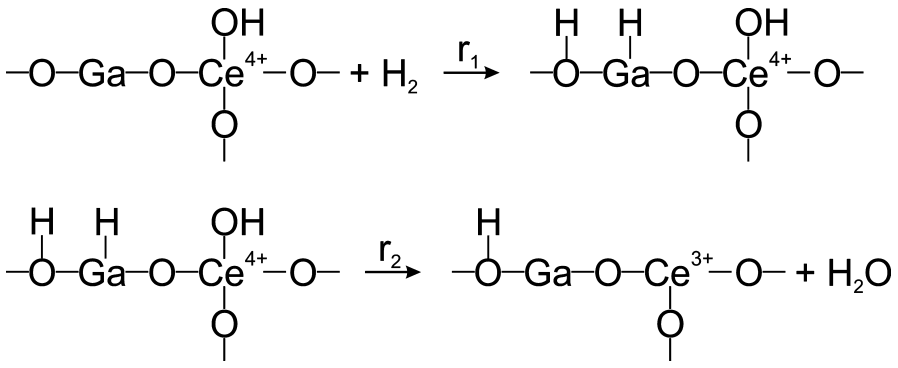

Figure 10. Surface reduction mechanism of Ce^{4+} to Ce^{3+} on the cerium−gallium mixed oxides.

for the reduction of Ce^{4+} to Ce^{3+} on the surface of cerium−gallium mixed oxides shown in Figure 10.

It is important to highlight that the experimental techniques used in this work are bulk techniques and, with some restrictions, mainly IR spectra can account for the (sub)surface reduction phenomena here described. Then, the proposed mechanism is restricted to the beginning of the reduction of the Ce−Ga mixed oxides.

The changes in the reaction rates of steps 1 and 2 (r_1 and r_2, respectively) may explain the traces of Ga−H in Figure 7. Below a given temperature, $r_1 > r_2$; that is, the formation of Ga−H bonds on the surface of Ce−Ga mixed oxide prevails over their consumption. Above 523 K, the consumption of atomic hydrogen begins to be dominated by the reduction of Ce^{4+} to Ce^{3+} ($r_2 > r_1$), and the surface concentration of Ga−H is reduced. At temperatures over 623 K, the concentration of Ce^{3+} in the material reaches a plateau and the Ga−H concentration increases with temperature. In this way, it is assumed that the activation energy of step 1 is lower than the one of step 2 (Figure 10).

The DRIFT results shown in Figure 9 are consistent with the proposed mechanism. When introducing a flow of H_2 to the oxidized Ce75Ga25 at 623 K, the fast growth of the signal of Ce^{3+} can be observed. Once the concentration of Ce^{3+} stabilizes, after approximately 2 min, the formation of Ga−H species begins. At this temperature, the rate of Ce^{4+} reduction, that is, the rate of Ga−H consumption (r_2), is faster than the formation of Ga−H species. Only the Ce^{3+} formation is observed at the beginning of the experiment. However, after reaching a pseudo-steady-state concentration of Ce^{3+}, the Ga−H species can be detected and their concentration increases with time.

In the isothermal experiment at 523 K, the Ga−H signal increases instantaneously to a maximum value and then drops as the concentration of Ce^{3+} arises; that is, Ga−H species are consumed in the cerium reduction process and the concentration of Ga−H stabilizes as does the one of Ce^{3+}. It is suggested that the lower Ga−H concentration, after the maximum, reached during the pseudo-steady-state can be explained if it is assumed that during this reduction process the oxide surface is modified in such a way that the number of surface sites able to adsorb dissociatively the hydrogen molecule is reduced: a saturation of surface O (by the formation of OH groups) has to occur by blocking the Ga−O pair needed for H_2 dissociation. It is then logical to expect that, at higher temperature, the unblocking of those sites could take place by H_2O desorption (by combination of two OH surface groups), and more Ga−H species can be generated (see Figure 7 at $T > 623$ K).

In order to further confirm the proposed mechanism and the role of Ce^{3+}, two additional isothermal DRIFT experiments were carried out by exposing the Ce75Ga25 sample containing only Ce^{3+} but not Ga−H species to molecular hydrogen. To obtain such a material, the Ce75Ga25 sample was previously reduced under H_2 flow, and then, the sample was purged with He (Ga−H surface species are labile and desorb H_2 by simple evacuation at this temperature). Thus, we obtained a reduced Ce75Ga25 sample, at 523 or 623 K, where only the IR signal of Ce^{3+} was detected after purging with He, while the Ga−H species vanished (similar to the upper trace at 723 K in Figure 6 for the Ce75Ga25 sample). When the previously reduced and swept sample was exposed to a flow of H_2, either at 523 or 623 K, an instantaneous production of Ga−H species was observed (see Figure 11). The Ga−H concentration reached a value

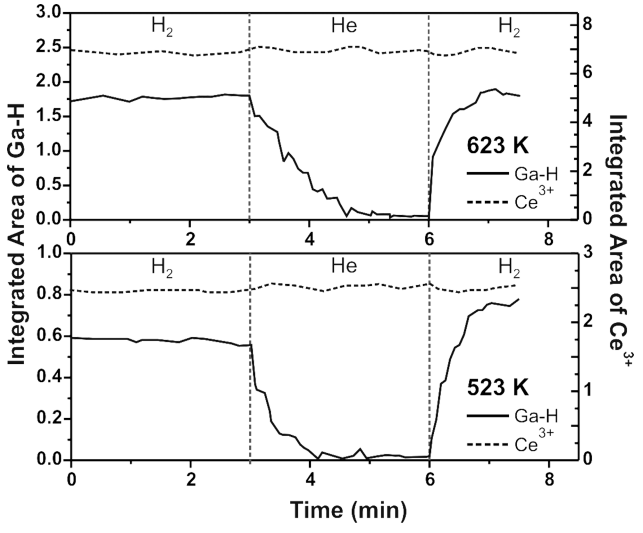

Figure 11. Isothermal evolution of the concentration of the Ce^{3+} and Ga−H species under flowing He and H_2 through the reduced Ce75Ga25 sample in the DRIFT cell.

similar to the one attained under the pseudo-steady-state condition (14 min) in the previously described DRIFT experiments carried out on the oxidized Ce75Ga25 sample at each temperature (Figure 9). Simultaneously, the Ce^{3+} concentration continued constant. Once the Ce^{3+} concentration achieves its pseudo-steady-state condition, molecular hydrogen dissociation occurs on gallium sites, and the prompt Ga−H regeneration is the only phenomenon that can be

dx.doi.org/10.1021/jp400285b | J. Phys. Chem. C 2013, 117, 8822−8831

expected, since the activation energy of hydrogen dissociation on gallium sites was assumed to be lower than the one of the reduction of Ce^{4+} to Ce^{3+}.

The proposed global mechanism for the surface reduction of Ce−Ga mixed oxides in Figure 10 can explain the different experimental results shown above. It is suggested that the role of gallium cations is to facilitate the hydrogen molecule dissociation to give atomic hydrogen, which further reacts with O atoms bonded to Ce^{4+} and Ga^{3+} cations to finally release water and to leave Ce^{3+}. In other words, and at the beginning, this is a gallium-assisted reduction mechanism, in which gallium cations behave "like" metals which are able to dissociate H_2 (the limiting step of the surface reduction process by H_2 in pure ceria), decreasing the temperature of reduction of pure CeO_2, as is the case of Rh/CeO_2.[39] Simultaneously, the extent of the reduction seems to be associated with the easy removal of O of Ce−O−Ga bonds, as is suggested by the theoretical calculations.

Temperature Programmed Oxidation. The O_2-TPO results obtained by IR spectroscopy indicate that Ce^{3+} is oxidized immediately to Ce^{4+} both in pure cerium oxide and the mixed oxide after the reduced and evacuated samples are exposed to O_2 at 300 K (see upper traces in Figure 6 for CeO_2 and Ce75Ga25, which depicts the identical results at 723 K). The results of *in situ* XRD show that, after exposing the prereduced sample Ce75Ga25 to O_2 and subsequently sweeping under a flow of He, the expansion of the lattice parameter recovers its original value. During the O_2-TPO, the lattice parameter expansion obtained is that expected by simple heating of the sample. The results obtained by both techniques are consistent and indicate that the reoxidation with O_2, both on Ce75Ga25 and CeO_2, is almost complete, even at 300 K.

In contrast, H_2O-TPO shows a different behavior for both materials. Figure 12 shows the variation of the integrated

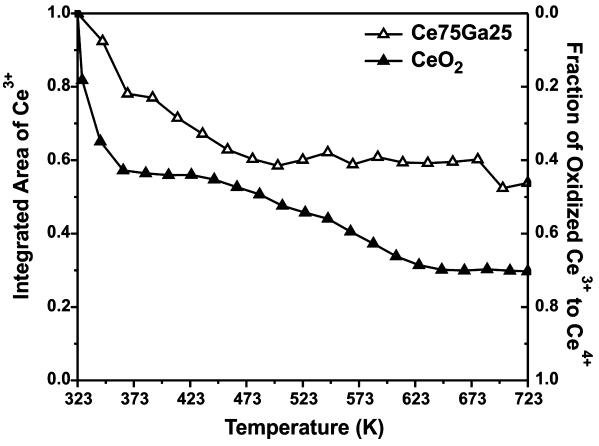

Figure 12. Normalized IR integrated areas of the Ce^{3+} signal ($^2F_{5/2} \rightarrow {}^2F_{7/2}$) as a function of the temperature during the H_2O-TPR experiment.

intensity of the IR signal corresponding to Ce^{3+} for CeO_2 and Ce75Ga25 samples during H_2O-TPO experiments. It is noted that there is a partial oxidation of Ce^{3+} to Ce^{4+} in both materials, because even at 723 K the band at 2127 cm^{-1} still persists. However, the fraction of Ce^{3+} oxidized to Ce^{4+} is approximately 50% higher on pure ceria than on Ce75Ga25 (70 and 45%, respectively). In other words, it is easier to reoxidize pure ceria than the mixed oxide.

Figure 13 shows the expansion of the lattice parameter for the H_2O-TPR measured by *in situ* XRD on Ce75Ga25 with the

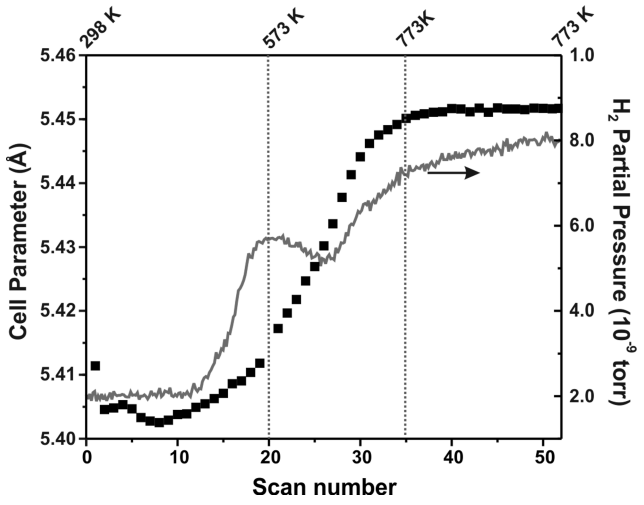

Figure 13. Thermal evolution of the lattice parameter (filled squares) and of the H_2 release (full line) measured by in situ XRD and MS, respectively, on Ce75Ga25 during the H_2O-TPR experiments.

simultaneous release of H_2 expected for this oxidation process. However, the observed lattice parameter is equal to 5.452 Å during the oxidation with H_2O at 773 K, that is, reaching a lattice parameter of ∼0.02 Å lower than the lattice increase shown for the highly reduced sample in H_2 or ∼0.04 Å higher than the expected value for the fully oxidized sample in O_2 at the same temperature (see vis à vis 5.475 or 5.412 Å, full or open symbols, in Figure 8, respectively). The incomplete reoxidation by water in the Ce75Ga25 is confirmed. If it is assumed that the lattice parameter is linearly correlated to the amount of oxygen vacancies in the oxide,[36] only about 50% (0.02/0.04) of the Ce^{3+} reoxidation can be estimated, in close agreement with the 45% found during the H_2O-TPR by IR.

These facts seem to point to a higher global activation energy for the reoxidation of the reduced cerium−gallium mixed oxides by water as compared to reduced ceria.

CONCLUSIONS

OSC, H_2-TPR, and XANES measurements show that doping CeO_2 with gallium markedly increases the reducibility of ceria. The XANES Ga K-edge spectrum of ceria−gallia samples shows that a change in the oxidation state of Ga^{3+} is undetectable even after exposing the sample to H_2 at temperatures up to 623 K. The DFT calculations verify the higher reducibility of the gallium-doped system with respect to the pure materials and point to important local distortions in the lattice as responsible for the unique redox property of the mixed oxide. The non-isothermal and isothermal reduction by molecular hydrogen was followed by infrared spectroscopy, and the evolution of the Ce^{3+} and Ga−H IR signals allows us to postulate a global two-step surface reduction mechanism that involves the participation of Ga^{3+} cations in the gallium−cerium mixed oxide. The H_2 is dissociatively chemisorbed to give Ga−H surface species, which are responsible for the facile reduction of Ce^{4+} to Ce^{3+}.

The O_2-TPO results obtained by in situ IR and XRD indicate that the Ce^{3+} of reduced samples is oxidized immediately to Ce^{4+} in both CeO_2 and the gallium−cerium mixed oxide when

dx.doi.org/10.1021/jp400285b | J. Phys. Chem. C 2013, 117, 8822−8831

exposed to O_2 at 300 K. The H_2O-TPO experiments showed that the reoxidation of Ce^{3+} to Ce^{4+} is partial in both materials; however, the reoxidized fraction of Ce^{3+} is 50% higher on pure ceria than on cerium−gallium mixed oxide.

The proposed reduction mechanism on the gallium−ceria samples and the lower oxidation power observed for water, as compared to oxygen, may help in the future to gain a better understanding of catalytic redox processes involving mixed oxides of ceria.

AUTHOR INFORMATION

Corresponding Author

*E-mail: abonivar@santafe-conciet.gov.ar. Fax: 54(342) 4550944. Phone: 54(342)4559175.

Present Address

[○]Instituto de Catálisis y Petroleoquímica, CSIC, Spain.

Notes

The authors declare no competing financial interest.

ACKNOWLEDGMENTS

This work has been financed by Eulanest 042, PME 2006 311, CAID 2009 J379, and MINCyT-ECOS A09E01. The work at BNL was financed by the US DOE, Office of BES (DE-AC02-98CH10086). M.C. and F.T. are grateful to HPC GENCI-CINES/IDRIS (grant 2011-x2011082131) and the CCRE-DSI of Université P. M. Curie for computational resources.

REFERENCES

(1) Trovarelli, A. *Catalysis by Ceria and Related Materials*; Catalytic Science Series, Vol. 2; Imperial College Press: London, 2002.

(2) Xiaolan, S.; Nan, J.; Yukun, L.; Dayu, X.; Guanzhou, Q. Synthesis and Characterization of Y-Doped Mesoporous CeO_2 Using a Chemical Precipitation Method. *J. Rare Earths* **2007**, *25*, 428−433.

(3) Varez, A.; Garcia-Gonzalez, E.; Jolly, J.; Sanz, J. Structural Characterization of $Ce_{1-x}Zr_xO_2$ ($0 \le x \le 1$) Samples Prepared at 1650 °C by Solid State Reaction: A Combined TEM and XRD Study. *J. Eur. Ceram. Soc.* **2007**, *27*, 3677−3682.

(4) Burch, R. Gold Catalysts for Pure Hydrogen Production in the Water-Gas Shift Reaction: Activity, Structure and Reaction Mechanism. *Phys. Chem. Chem. Phys.* **2006**, *8*, 5483−5500.

(5) Barrio, L.; Zhou, G.; González, I. D.; Estrella, M.; Hanson, J.; Rodriguez, J. A.; Navarro, R. M.; Fierro, J. L. G. In Situ Characterization of Pt Catalysts Supported on Ceria Modified TiO_2 for the WGS Reaction: Influence of Ceria Loading. *Phys. Chem. Chem. Phys.* **2012**, *14*, 2192−2202.

(6) Xu, W.; Si, R.; Senanayake, S. D.; Llorca, Y.; Idriss, H.; Stacchiola, D.; Hanson, J. C.; Rodriguez, J. A. In Situ Studies of CeO_2-Supported Pt, Ru, and Pt−Ru Alloy Catalysts for the Water−Gas Shift Reaction: Active Phases and Reaction Intermediates. *J. Catal.* **2012**, *291*, 117−126.

(7) Park, J. B.; Graciani, J.; Evans, J.; Stacchiola, D.; Senanayake, S. D.; Barrio, L.; Liu, P.; Sanz, J. F.; Hrbek, J.; Rodriguez, J. A. Gold, Copper, and Platinum Nanoparticles Dispersed on CeOx/TiO2(110) Surfaces: High Water-Gas Shift Activity and the Nature of the Mixed-Metal Oxide at the Nanometer Level. *J. Am. Chem. Soc.* **2010**, *132*, 356−363.

(8) Cosandey, F.; Madey, T. E. Growth, Morphology, Interfacial Effects and Catalytic Properties of Au on TiO_2. *Surf. Rev. Lett.* **2001**, *8*, 73−93.

(9) Bamwenda, G. R.; Tsubota, S.; Nakamura, T.; Haruta, M. The Influence of the Preparation Methods on the Catalytic Activity of Platinum and Gold Supported on TiO_2 for CO Oxidation. *Catal. Lett.* **1997**, *44*, 83−87.

(10) Valden, M.; Lai, X.; Goodman, D. W. Onset of Catalytic Activity of Gold Clusters on Titania with the Appearance of Nonmetallic Properties. *Science* **1998**, *281*, 1647−1650.

(11) Bond, G. C.; Louis, C.; Thompson, D. T. *Catalysis by Gold*; Catalytic Science Series, Vol. 6; World Scientific Publishing Co: London, 2006.

(12) Park, J. B.; Graciani, J.; Evans, J.; Stacchiola, D.; Ma, S.; Liu, P.; Nambu, A.; Fernández-Sanz, J.; Hrbek, J.; Rodriguez, J. A. High Catalytic Activity of $Au/CeO_x/TiO_2$ (110) Controlled by the Nature of the Mixed-Metal Oxide at the Nanometer Level. *Proc. Natl. Acad. Sci. U.S.A.* **2009**, *106*, 4975−4980.

(13) Deng, W.; Flytzani-Stephanopoulos, M. On the Issue of the Deactivation of Au−Ceria and Pt−Ceria Water−Gas Shift Catalysts in Practical Fuel-Cell Applications. *Angew. Chem., Int. Ed.* **2006**, *45*, 2285−2289.

(14) Collins, S.; Finos, G.; Alcántara, R.; del Rio, E.; Bernal, S.; Bonivardi, A. Effect of Gallia Doping on the Acid−Base and Redox Properties of Ceria. *Appl. Catal., A* **2010**, *388*, 202−210.

(15) Finos, G.; Collins, S.; Blanco, G.; del Rio, E.; Cíes, J. M; Bernal, S.; Bonivardi, A. Infrared Spectroscopic Study of Carbon Dioxide Adsorption on the Surface of Cerium−Gallium Mixed Oxides. *Catal. Today* **2012**, *180*, 9−18.

(16) Vecchietti, J.; Collins, S.; Delgado, J. J.; Małecka, M.; del Río, E.; Chen, X.; Bernal, S.; Bonivardi, A. Gold Catalysts Supported on Cerium−Gallium Mixed Oxide for the Carbon Monoxide Oxidation and Water Gas Shift Reaction. *Top. Catal.* **2011**, *54*, 201−209.

(17) Wang, X. Q.; Hanson, J. C.; Frenkel, A. I.; Kim, J. Y.; Rodríguez, J. A. Time-resolved Studies for the Mechanism of Reduction of Copper Oxides with Carbon Monoxide: Complex Behavior of Lattice Oxygen and the Formation of Suboxides. *J. Phys. Chem. B* **2004**, *108*, 13667−13673.

(18) Ravel, B.; Newville, M. ATHENA, ARTEMIS, HEPHAESTUS: Data Analysis for X-ray Absorption Spectroscopy Using IFEFFIT. *J. Synchrotron Radiat.* **2005**, *12*, 537−541.

(19) Kresse, G.; Furthmüller, J. Efficient Iterative Schemes for Ab Initio Total-Energy Calculations Using a Plane-Wave Basis Set. *Phys. Rev. B* **1996**, *54*, 11169−11186.

(20) Kresse, G.; Hafner, J. Ab Initio Molecular Dynamics for Liquid Metals. *Phys. Rev. B* **1993**, *47*, 558−561.

(21) Kresse, G.; Hafner, J. Ab Initio Molecular-Dynamics Simulation of the Liquid-Metal−Amorphous-Semiconductor Transition in Germanium. *Phys. Rev. B* **1994**, *49*, 14251−14269.

(22) Kresse, G.; Hafner, J. Norm-Conserving and Ultrasoft Pseudopotentials for First-Row and Transition Elements. *J. Phys.: Condens. Matter* **1994**, *6*, 8245−8257.

(23) Kresse, G.; Joubert, D. From Ultrasoft Pseudopotentials to the Projector Augmented-Wave Method. *Phys. Rev. B* **1999**, *59*, 1758−1775.

(24) Overbury, S. H.; Huntley, D. R.; Mullins, D. R.; Glavee, G. N. XANES Studies of the Reduction Behavior of $(Ce_{1-y}Zr_y)O_2$ and $Rh/(Ce_{1-y}Zr_y)O_2$. *Catal. Lett.* **1998**, *51*, 133−138.

(25) Rodriguez, J. A.; Wang, X.; Hanson, J. C.; Liu, G. The Behavior of Mixed-Metal Oxides: Structural and Electronic Properties of $Ce_{1-x}Ca_xO_2$ and $Ce_{1-x}Ca_xO_{2-x}$. *J. Chem. Phys.* **2003**, *119*, 5659−5669.

(26) Jiang, Y.; Adams, J. B.; van Schilfgaarde, M.; Sharma, R.; Crozier, P. A. Theoretical Study of Environmental Dependence of Oxygen Vacancy Formation in CeO_2. *Appl. Phys. Lett.* **2005**, *87*, 141917−141919.

(27) Quaino, P.; Syzgantseva, O.; Siffert, L.; Tielens, F.; Minot, C.; Calatayud, M. Unravelling the Enhanced Reactivity of Bulk CeO_2 Doped with Gallium: A Periodic DFT Study. *Chem. Phys. Lett.* **2012**, *519*−*520*, 69−72.

(28) Calatayud, M.; Markovits, A.; Menetrey, M.; Mguig, B.; Minot, C. Adsorption on Perfect and Reduced Surfaces of Metal Oxides. *Catal. Today* **2003**, *85*, 125−143.

(29) Calatayud, M.; Markovits, A.; Minot, C. Electron-Count control on Adsorption upon Reducible and Irreducible Clean Metal-Oxide Surfaces. *Catal. Today* **2004**, *89*, 269−278.

(30) Binet, C.; Badri, A.; Lavalley, L.-C. A Spectroscopic Characterization of the Reduction of Ceria from Electronic Transitions of Intrinsic Point Defects. *J. Phys. Chem.* **1994**, *98*, 6392−6398.
(31) Binet, C.; Daturi, M.; Lavalley, J.-C. IR Study of Polycrystalline Ceria Properties in Oxidised and Reduced States. *Catal. Today* **1999**, *50*, 207−225.
(32) Tabakova, T.; Boccuzzi, F.; Manzoli, M.; Andreeva, D. FTIR Study of Low-Temperature Water-Gas Shift Reaction on Gold/Ceria Catalyst. *Appl. Catal., A* **2003**, *252*, 385−397.
(33) Meunier, F. C.; Tibiletti, D.; Goguet, A.; Reid, D.; Burch, R. On the Reactivity of Carbonate Species on a Pt/CeO_2 Catalyst under Various Reaction Atmospheres: Application of the Isotopic Exchange Technique. *Appl. Catal., A* **2005**, *289*, 104−112.
(34) Collins, S. E.; Baltanás, M. A.; Bonivardi, A. L. Hydrogen Chemisorption on Gallium Oxide Polymorphs. *Langmuir* **2005**, *21*, 962−970.
(35) Collins, S. E.; Baltanás, M. A.; Garcia Fierro, J. L.; Bonivardi, A. L. Gallium−Hydrogen Bond Formation on Gallium and Gallium−Palladium Silica-Supported Catalysts. *J. Catal.* **2002**, *211*, 252−264.
(36) Chiang, H. W.; Blumenthal, R. N.; Fournelle, R. A. A High Temperature Lattice Parameter and Dilatometer Study of the Defect Structure of Nonstoichiometric Cerium Dioxide. *Solid State Ionics* **1993**, *66*, 85−95.
(37) Tyagi, A. K.; Ambekar, B. R.; Mathews, M. D. Simulation of Lattice Thermal Expansion Behaviour of $Th_{1-x}Pu_xO_2$ ($0.0 \leq x \leq 1.0$) using CeO_2 as a Surrogate Material for PuO_2. *J. Alloys Compd.* **2002**, *337*, 277−281.
(38) Kossoy, A.; Frenkel, A. I.; Feldman, Y.; Wachtel, E.; Milner, A.; Lubomirsky, I. The Origin of Elastic Anomalies in Thin Films of Oxygen Deficient Ceria, CeO_{2-x}. *Solid State Ionics* **2010**, *181*, 1473−1477.
(39) El Fallah, J.; Boujana, S.; Dexpert, H.; Kiennemann, A.; Majerus, J.; Touret, O.; Villain, F.; Le Normand, F. Redox Processes on Pure Ceria and on Rh/CeO_2 Catalyst Monitored by X-Ray Absorption (Fast Acquisition Mode). *J. Phys. Chem.* **1994**, *98*, 5522−5533.